JCTC Journal of Chemical Theory and Computation

Article

pubs.acs.org/JCTC

Nuclear Quantum Effects in Water: A Multiscale Study

Sebastian Fritsch, Raffaello Potestio,* Davide Donadio,* and Kurt Kremer

Max Planck Institute for Polymer Research, Ackermannweg 10, 55128 Mainz, Germany

Supporting Information

ABSTRACT: We outline a method to investigate the role of nuclear quantum effects in liquid water making use of a force field derived from ab initio simulations. Starting from a first-principles molecular dynamics simulation, we obtain an effective force field for bulk liquid water using the force-matching technique. After validating that our effective model reproduces the key structural and dynamic properties of the reference system, we use it to perform path integral simulations to investigate the role played by nuclear quantum effects on bulk water, probing radial distribution functions, vibrational spectra, and hydrogen bond fluctuations. Our approach offers a practical route to derive ab initio quality molecular models to study quantum effects at a low computational cost.

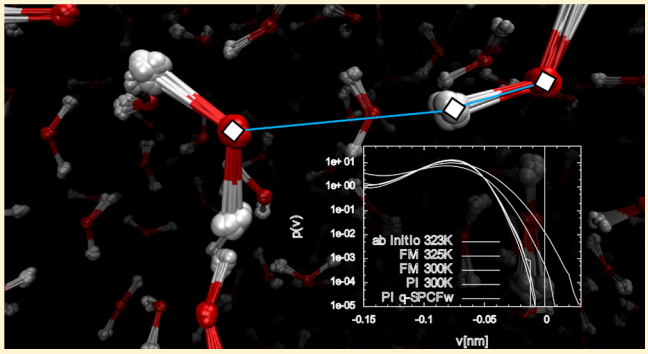

1. INTRODUCTION

Nuclear quantum effects in liquid water are still under study 30 years after the first pioneering simulations by Kuharski and Rossky.[1] Most studies find that the quantum behavior of hydrogen atoms leads to a softening of the liquid structure,[2] but also the counterintuitive opposite effect has been proposed.[3] In order to obtain quantitatively reliable results, one faces the problem of selecting an appropriate model to describe intermolecular and intramolecular interactions. Empirical models allow numerical simulations of water at fairly low computational cost, but they are often parametrized on experimental observables,[4−6] and therefore they intrinsecally include nuclear quantum effects. Performing quantum dynamics simulations with these models, for example using Feynman's Path Integral (PI) formalism, would lead to a double counting of quantum effects. To overcome this issue, a two-step procedure of refitting parameters was suggested in refs 7 and 8. Alternatively, it is possible to fit empirical potentials to high level data, typically calculated for small water clusters.[9−17] Although this approach has been very successful, for example, in accurately predicting the binding energy of water clusters,[17] a potential fitted on cluster models has to contain explicit polarization to be transferable to condensed phases. In addition, such polarizable models imply relatively complicated functional forms and high computational cost, due to their iterative formulation.

A possible alternative is to perform parameter-free, first-principles simulations including ionic quantum effects. Marx et al. performed *ab initio* PI molecular dynamics (PIMD),[18,19] in the framework of density functional theory (DFT), to study the solvation of an excess proton and of the hydroxide ion in water.[20,21] A similar approach was used by Morrone and Car to probe quantum effects in water,[22] showing that the inclusion of nuclear quantum effects improves the agreement of DFT-based simulations with the experimental structure determined by X-ray and neutron scattering.[23−25] Although accurate and predictive, a parameter-free approach based on first-principles molecular dynamics (MD) simulations has an extremely high computational cost, which limits the size of systems that can be sampled to less than ∼100 water molecules and the time to a few tens of picoseconds. Such limitations hinder the application of *ab initio* PIMD to heterogeneous systems, such as air−water interfaces or biological environments, which have been experimentally investigated in recent times.[26−29]

In this work, we develop a systematic approach to obtain a computationally efficient quantum model of water, from a reference first-principles (DFT) MD simulation. This model can be used to overcome the limits of first-principles simulations in terms of time and length scales, thus making it possible to perform large scale simulations explicitly including the nuclear quantum effects. Within our fitting scheme, intramolecular and intermolecular interactions are fitted using the force-matching (FM) method, which had been previously used to extract effective interactions for use in classical MD[30] based on reference Car−Parrinello MD[31] simulations. The model functions used for FM are optimized to reproduce the correct local bulk structure and dynamical properties. The interactions are simple tabulated two-body nonbonded potentials and tabulated, flexible intramolecular interactions, which are still very inexpensive to compute in most MD packages. Long-range Coulombic interactions are taken into account effectively in the nonbonded interactions, thus avoiding the explicit assignment of charges. To overcome structural

Received: December 4, 2013
Published: January 13, 2014

deficits that are visible in the FM-based classical interaction, we introduce corrections using the iterative Boltzmann inversion (IBI) scheme.[32]

We apply this multiscale approach to evaluate nuclear quantum effects on the structure of water at room temperature as obtained from a first-principles MD, employing the widely used generalized gradient approximation (GGA) functional by Perdew, Burke, and Ernzerhof (PBE).[33] In contrast with standard flexible water force fields,[6] the FM potential derived in this work reproduces very well the vibrational properties of liquid water, including the broad and complex H−O stretching band. With this tool, which is completely general and not limited to the specific system, not only can we investigate the impact of nuclear quantum effects on the structure but we can also utilize centroid molecular dynamics (CMD)[34] to assess quantum effects on the dynamic and vibrational properties of water.

2. METHODS

2.1. First Principles Molecular Dynamics. The first-principles simulations of heavy water (D_2O) were performed using the CP2K-Quickstep simulation package.[35] Following the Quickstep approach, electronic wave functions are expanded on a localized basis set, and an auxiliary plane waves basis set is used to represent the charge density in reciprocal space. In the real space, the electronic Kohn−Sham wave functions are expanded on a TZVP2 localized basis set,[36] and the cutoff for the auxiliary plane waves basis set was set to 280 Ry. The PBE generalized gradient approximation (GGA) is employed for the exchange and correlation functional.[33] All nuclei are described as classical point particles, and the dynamics was evolved integrating Newton's equations of motion.

In this framework, we simulated a system of 128 heavy water molecules at a density of 1.1 g/cm^3 in a cubic box with side length l = 1.568 nm. Prior to the production microcanonical (NVE) runs, the simulations were equilibrated in the NVT ensemble at T = 320 K for 10 ps using stochastic velocity rescaling.[37] The temperature in the 10 ps production NVE data set was found to be $T = 325 \pm 0.8$ K. Note that the simulations were performed at 320 K instead of room temperature in order to improve the efficiency of the sampling, since otherwise the self-diffusion coefficient of water is limited by both finite size effects and the approximations in the interactions introduced by GGA.[38,39] In the following, we assume that the effective interactions derived from this data set are transferable to room temperature.

2.2. Multiscale Coarse-Graining. To derive an effective interaction from the first-principles MD simulation, we used the force matching (FM) method[40] with modifications as suggested in the Multiscale Coarse-Graining (MSCG) technique.[30,41,42] In this approach, effective interactions between the atoms are obtained by parametrizing a set of model functions to reproduce the *average* total force on each atom. The best possible fit of the average force is determined in a least-squares minimization procedure, which has to contain a sufficient amount of frames from the reference trajectory to represent the ensemble average. The most general form of the model force is given by

$$\mathbf{F}^{\mathrm{FM}} = \mathbf{F}^{\mathrm{FM}}(f_1, ..., f_N) \tag{1}$$

where the coefficients $f_1,...f_N$ are to be determined in the least-squares minimization procedure. In the following, forces on deuterium (D) and oxygen (O) atoms are discussed, as we are first performing FM on a heavy water first-principles reference simulation. For the nonbonded (nb) interactions between D−D, D−O, and O−O, we choose spherical-symmetric forces

$$\mathbf{F}_\alpha^{\mathrm{nb}} = \sum_\beta F_{\alpha\beta}^{\mathrm{nb}}(r_{\alpha\beta})\hat{\mathbf{r}}_{\alpha\beta} \tag{2}$$

where the indices α, β = D, O denote the different combinations of atom types and the function $F_{\alpha\beta}^{\mathrm{nb}}$ is represented by cubic splines (hence, the minimization procedure is carried out with respect to the cubic splines coefficients[30]). The internal interactions are represented by a D−O bonded force:

$$\mathbf{F}^{\mathrm{b}} = F^{\mathrm{b}}(r_{\mathrm{OD}})\hat{\mathbf{r}}_{\mathrm{OD}} \tag{3}$$

and an angular term depending on the D−O−D bending angle θ:

$$\mathbf{F}^{\theta} = -\frac{\partial V}{\partial \theta}\frac{\partial \theta}{\partial \mathbf{r}_i} = F^{\theta}(\theta)\nabla_{\mathbf{r}_i}\theta \tag{4}$$

where i specifies the atom. The different contributions are defined additively:

$$\mathbf{F}_i^{I,\mathrm{FM}} = \mathbf{F}_i^{\mathrm{nb}} + \mathbf{F}_i^{\mathrm{b}} + \mathbf{F}_i^{\theta} \tag{5}$$

and I denotes the frame in the reference trajectory. The FM procedure is carried out by minimizing the difference between the model force $\mathbf{F}_i^{I,\mathrm{FM}}$ and instantaneous reference force $\mathbf{F}_i^{I,\mathrm{REF}}$:

$$\chi^2 = \frac{1}{3N_I N_{\mathrm{AT}}}\sum_I^{N_I}\sum_i^{N_{\mathrm{AT}}} |\mathbf{F}_i^{I,\mathrm{REF}} - \mathbf{F}_i^{I,\mathrm{FM}}|^2 \tag{6}$$

where N_I is the number of frames in the reference trajectory and N_{AT} the number of atoms of a given type (details of the procedure can be found in ref 42). The FM algorithm was used as implemented in the VOTCA[43] software package.

2.3. Iterative Bolzmann Inversion. As will be shown below, it is beneficial to the present study to apply an additional correction in terms of the iterative Boltzmann inversion (IBI).[32] This approach, which is commonly used in the context of coarse-graining (reduction of degrees of freedom), is aimed at exactly reproducing the reference two-body correlation function $g(r)$. A correction to the potential is defined which is based on the difference between the current approximation to the 2-body PMF $w^{(i)}(r) = -k_{\mathrm{B}}T \ln g^{(i)}(r)$ and the reference $w^{(\mathrm{REF})}(r)$

$$\Delta U^{(i)}(r) = s(w^{(\mathrm{REF})}(r) - w^{(i)}(r)) \tag{7}$$

$$= s(k_{\mathrm{B}}T \ln[g^{(i)}(r)/g^{(\mathrm{REF})}(r)]) \tag{8}$$

where s is a scaling factor controlling the stability. An iterative procedure is then performed, where a simulation with the initial $U^{(1)} = w^{(\mathrm{REF})}$ obtained by integration of the FM forces is used as a starting guess. The procedure is repeated with a corrected potential using eq 8 until convergence of the $g^{(i)}(r)$. The advantage of this method is that it will always find a potential which reproduces the reference structure. However, since IBI assumes that the difference is based on a pair correlation, three-body or higher order correlations are not taken into account. Here, we will use IBI only as a small correction to the nonbonded term to improve the structural deficiencies of the FM solution.

The interaction ranges, shown in Table 1, were chosen based on the radial distribution function $g(r)$ as calculated from the

dx.doi.org/10.1021/ct4010504 | J. Chem. Theory Comput. 2014, 10, 816−824

Table 1. Ranges of the Tabulated Potentials Used for Force Matching

	r_{min} [nm]	r_{max} [nm]	Δr [nm]	r^{fit}_{min} [nm]	r^{fit}_{max} [nm]
V^{nb}_{OO}	0.24	0.78	0.01	0.28	
V^{nb}_{HO}	0.14	0.78	0.01	0.17	
V^{nb}_{HH}	0.16	0.78	0.01	0.20	
V^{b}_{HO}	0.09	0.11	0.001	0.093	0.107
V^{b}_{HOH}	1.57 rad	2.1 rad	0.01 rad	full range	
V^{b}_{HH}	0.142	0.175	0.01	full range	

first-principles reference simulation. Long range interactions, such as electrostatics, were not considered explicitly; rather, they were effectively included in the nonbonded forces. The advantages are a simpler and computationally more efficient treatment of the interactions, while still maintaining all the information on local structure and dynamics, which is the focus of this study.

2.4. Path Integral Formalism: Equilibrium Simulations and Centroid Molecular Dynamics. The inclusion of nuclear delocalization effects in the classical simulations employing the force-matched potential was performed making use of Feynman's Path Integral[44] formulation of Quantum Mechanics. In this formalism, the partition function of a quantum system is expressed in terms of *classical* degrees of freedom: a quantum particle is mapped onto a closed necklace, or *ring polymer*, of beads coupled to first neighbors via harmonic springs of elastic constant $m\omega_0^2$, where $\omega_0 = 1/(\hbar\beta_P)$ and $\beta_P = 1/(Pk_BT)$ is the rescaled inverse temperature, k_B is Boltzmann's constant, and $\hbar$ is Planck's constant. The partition function of the system can be written as

$$Z = \lim_{P\to\infty} N(P) \int \mathcal{D}[x]\, \mathcal{D}[p]\, e^{-\beta_P H_P} \tag{9}$$

$$\mathcal{D}[p] \equiv dp_1 \cdots dp_P$$

$$H_P \equiv \sum_{l=1}^{P} \left\{ \frac{p_l^2}{2m} + m\omega_0^2 (x_l - x_{l+1})^2 + V(x_l) \right\}$$

where $N(P)$ is a P-dependent normalization constant. Each bead interacts with beads in other rings at the same imaginary time via the intermolecular potential V. Cyclic conditions in the sum are enforced, such that $x_{l+P} = x_l$.

In order to efficiently sample the polymer ring configurational space, the numerical integration of the equations of motion can be performed in the space of the noninteracting normal modes of the PI ring polymers $q_n = O^T_{nl} x_l$; the transformed Hamiltonian thus reads

$$H_P = \sum_{n=1}^{P} \left\{ \frac{p_n^2}{2\mu_n} + \frac{1}{2} m\omega_0^2 \lambda_n q_n^2 \right\} + \sum_{l=1}^{P} V(x_l) \tag{10}$$

where λ_n is the nth eigenvalue of the free ring Hamiltonian. The first eigenvalue $\lambda_1 = 0$ is related to the translational mode of the free ring, and the corresponding coordinate is proportional to the chain's center of mass. By construction, the masses μ_n do not affect the equilibrium properties and can be chosen arbitrarily; therefore, their value can be tuned to reduce the breadth of the frequency spectrum of the system, in order to accelerate and improve the exploration of the configurational space. Specifically, all frequencies of the free chain normal modes with $n = 1$ can be collapsed on the same value by setting $\mu_n = m\lambda_n$.

The trajectories generated by the Hamiltonian in eq 9 sample the correct configurational space of the system and can be used to extract equilibrium properties. On the other hand, they do not provide meaningful information about the real quantum dynamics of the system. The Centroid Molecular Dynamics (CMD) method, developed by Cao and Voth,[34] makes use of a concept introduced by Feynman, the *centroid*, to calculate approximate time-dependent correlation functions of the quantum system in the short-time regime. The centroid variable and its momentum are defined as the averages of the beads' corresponding quantities:

$$x_0 = \frac{1}{P}\sum_{l=1}^{P} x_l,\ p_0 = \frac{1}{P}\sum_{l=1}^{P} p_l \tag{11}$$

The probability density for the centroid coordinate is obtained from a constrained integration of the Boltzmann weight in eq 9:

$$\rho(x_c) = (2\pi\hbar) \lim_{P\to\infty} \left[\frac{mP}{2\pi\hbar^2\beta}\right]^{P/2} \int \mathcal{D}[x]\, \delta(x_c - x_0)\, e^{-\beta_P H_P} \tag{12}$$

Accordingly, we can compute an effective potential acting on the centroid position variables as $V_{eff}(x_c) = -k_BT \log(\rho(x_c))$. The underlying assumption of CMD is that the real quantum dynamics of the system is approximated by a Newtonian evolution of the centroid coordinates on the potential energy surface generated by the effective potential $V_{eff}(x_c)$. The corresponding equations of motion are given by

$$\dot{x}_c = \frac{p_c}{m} \tag{13}$$

$$\dot{p}_c = -\frac{dV_{eff}(x_c)}{dx_c} = F_{eff}(x_c) \tag{14}$$

$$F_{eff}(x_c) = \left\langle \frac{1}{P}\sum_{l=1}^{P} \frac{\partial V(x_l)}{\partial x_l} \right\rangle_{x_0 = x_c} \tag{15}$$

In eq 15, the average is performed with the constraint that the ring polymer's centroid is held fixed in x_c, which is a computationally expensive calculation. This limitation can be overcome by adiabatically decoupling the motion of the ring polymers' centers of mass from the internal fluctuations: rescaling the fictitious masses of the nonzero modes by a factor $\gamma^2 < 1$, i.e., setting $\mu'_{n\neq 0} = \gamma^2 m\lambda_n$, the internal dynamics of the rings evolves artificially faster than the centroids, while the latter follow the potential energy surface generated "on the fly" by the nonzero modes. Additionally, in order to provide a canonical sampling of the centroid force in eq 15, the noncentroid modes are coupled to a thermostat; in contrast, the dynamics of the centroids remains Newtonian. This strategy, that goes under the name of Adiabatic Centroid Molecular Dynamics (ACMD), has been shown[34] to provide a good approximation to the short- time quantum dynamics of the system and is exact in the harmonic limit for linear operators, for a free particle and in the high temperature limit.

3. RESULTS

3.1. Classical Model. As a first step of our procedure, effective interaction potentials were obtained using FM based

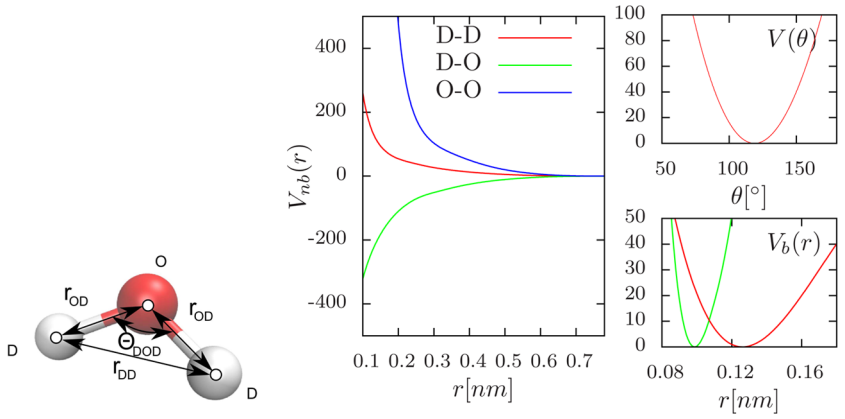

Figure 1. Potentials obtained by integrating the FM forces. The lower right plot shows both $V_b(r_{DO})$ (green) as well as $V_b(r_{DD})$ (red) bonded interactions. Potentials are in kJ/mol.

on the first-principles MD reference trajectory. From the total 16 ps first-principles simulation, 2.5 ps were considered equilibration and discarded. The remaining part was subdivided into 29 blocks of 0.5 ps containing 100 snapshots at an interval of 5 fs. The minimization in eq 6 was carried out for each block, and subsequently the average over all blocks was taken. In order to extrapolate to the unsampled regions at $r < r_{min}$, the force curves were fit with a power law of the form $f(r) \propto q/r^k$ for the D−D and D−O interactions and a reaction-field+VdW interaction of the form $f(r) \propto = q/\varepsilon_{RF}(1/r^2 - 2k_{RF}) + 12A/r^{13} + 6B/r^7$ for the O−O interaction. The fit included only points in the range $r_{min} \leq r_{min}^{fit}$ since no functional form for the entire range could be found. The ranges are specified in Table 1.

The potentials resulting from the integration of the FM forces (eq 2) are shown in Figure 1. The Coulombic part of the interaction manifestly dominates the overall shape of the nonbonded potentials; the D−O bonded interaction shows a pronounced anharmonicity, while the angular potential is harmonic in good approximation.

The best results were obtained when we considered a classical model employing angular $V(\theta)$ and bond $V_b(r_{DO})$ potentials, supplemented by an additional anharmonic tabulated potential $V_b(r_{DD})$, as shown in Figure 1. The reason is that with the additional D−D interaction, correlations between the stretching and bending modes are explicitly taken into account. This was verified by calculating the bond-angle correlations in classical simulations for force fields obtained without (FM) and with (FM-DD) additional D−D bonded interaction. The result is shown in Figure 2 where the two-dimensional distribution $p(\theta, r_{DO})$ is compared to the reference first-principles correlation. In the simulations employing the FM-DD force field, the agreement is considerably improved.

To asses how well the structural properties of the first-principles simulation are reproduced by the FM-DD potentials, we performed a classical MD simulation at the reference temperature of $T = 325$ K. This simulation was run for 1 ns using a time step of $\Delta t = 0.5$ fs. The temperature was controlled using a Langevin thermostat with a characteristic time constant $\tau_{Langevin} = 0.5$ ps. Figure 3 shows the radial distribution functions for D−D, D−O, and O−O including intramolecular contributions. The first-principles structure is in general well reproduced; however, some small deviations are visible especially in the D−D radial distribution function. This deviation is most likely due to the fact that the D−D bonded

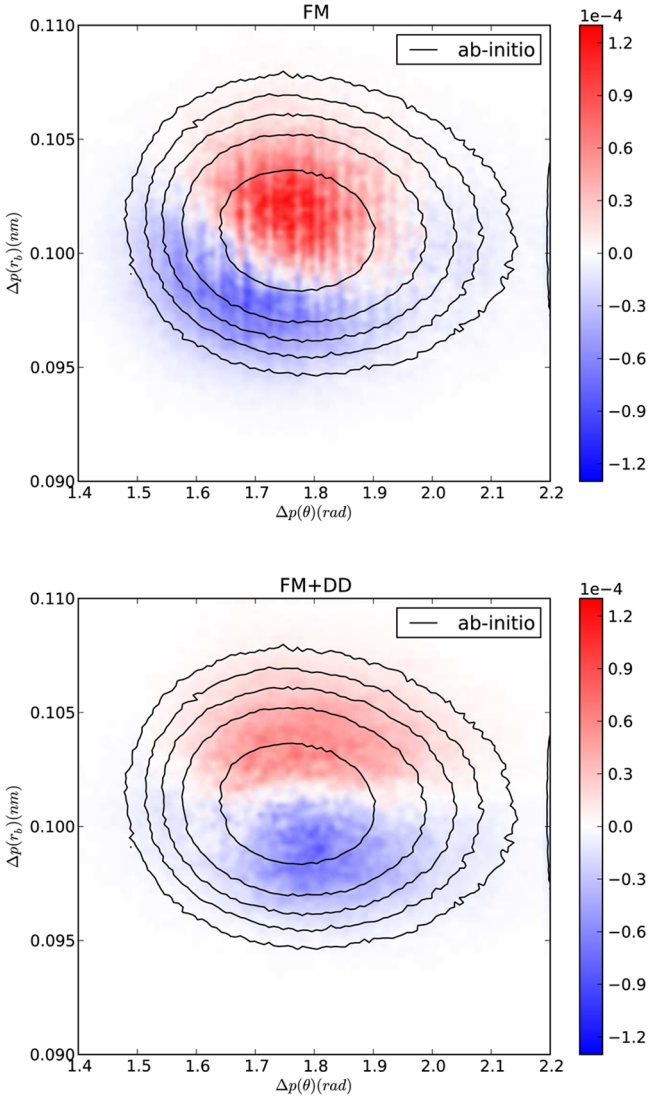

Figure 2. Comparison of bond-angle correlations without (upper plot) and with (lower plot) additional D−D interaction. Shown is the difference with respect to the distribution measured in the first-principles DFT simulation: $\Delta_p(r_{OD},\theta) = p_{FM}(r_{OD},\theta) - p_{DFT}(r_{OD},\theta)$.

and D−D nonbonded distributions overlap. Since only the total force per atom enters the FM algorithm, the contributions from

dx.doi.org/10.1021/ct4010504 | J. Chem. Theory Comput. 2014, 10, 816−824

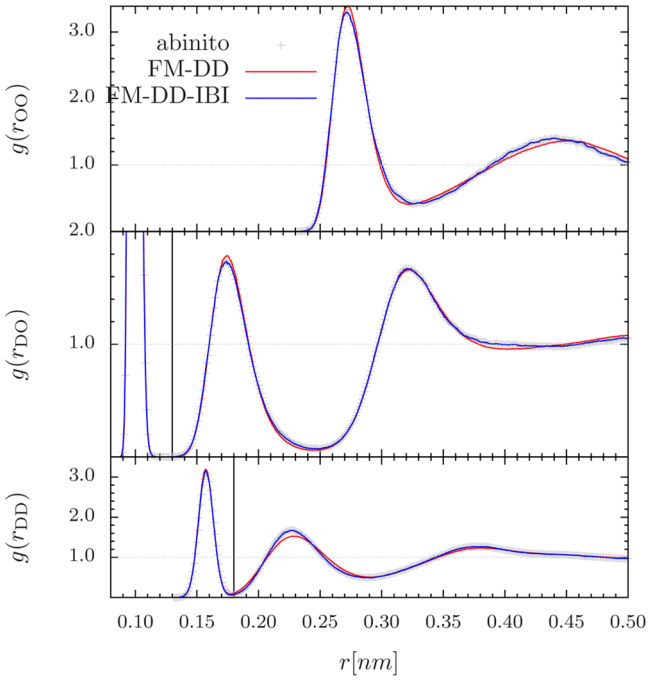

Figure 3. Radial distribution function of FM-DD and IBI corrected classical models (D_2O) compared to the ab initio reference simulation data at T = 325 K.

D−D bonded and nonbonded interactions cannot be distinguished; hence the balance between these contributions may have been unsatisfactorily reproduced. Further evidence for this is given by the shifted D−O−D bending frequency, which hints at a too low D−D bonded force (see following section, Dynamical Properties): a similar observation was already made in ref 30. Since it is beneficial for this study to exactly reproduce the reference structure in the classical MD simulation, an additional correction to the FM-DD potential was implemented, applying the IBI method as previously discussed. To this end, 70 IBI iterations were performed at a temperature of 325 K, each for a simulation length of 1 ns. Updates were performed for all nonbonded interaction types simultaneously in each step. The structure in the final iteration is shown in Figure 3, and the corrections to the FM-DD potential are shown in Figure 4. In essence, small corrections to the potential of about 1% (absolute changes of approximately $0.5k_BT$) are sufficient to achieve a very good agreement with the first-principles radial distribution functions. We will refer to the potential including IBI correction as FM-DD-IBI.

The structural properties of these force fields have been further investigated by measuring the distribution of an orientational order parameter as in ref 45, defined as

$$q_4 = 1 - \frac{3}{8}\sum_{j=1}^{3}\sum_{k=j+1}^{4}\left(\cos(\Psi_{jk}) + \frac{1}{3}\right)^2 \tag{16}$$

where $\Psi_{jk} = \arccos(\hat{\mathbf{r}}_{ij}\ \hat{\mathbf{r}}_{ik})$ is the angle between a selected oxygen atom i and the vectors connecting the oxygen position $\mathbf{r}_i$ to its four next neighbors $\mathbf{r}_j$ and $\mathbf{r}_k$ (with $j, k \leq 4$). The value 1/3 stems from the ideal tetrahedral angle ($\arccos(-1/3)$). In a perfect tetrahedral (ice I_h) arrangement, q_4 = 1; whereas in an ideal gas, q_4 = 0. The order parameter can therefore measure to what extent the liquid has an "on average" hexagonal arrangement. The distribution of q_4 values calculated from

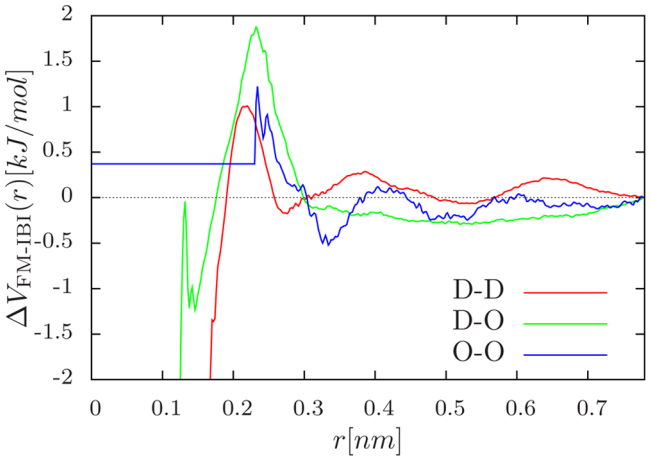

Figure 4. Changes in potential introduced by the IBI correction compared to the FM-DD potential.

MD simulation are shown in Figure 5. For the first-principles reference simulation (D_2O), a single peak at around 0.9 is

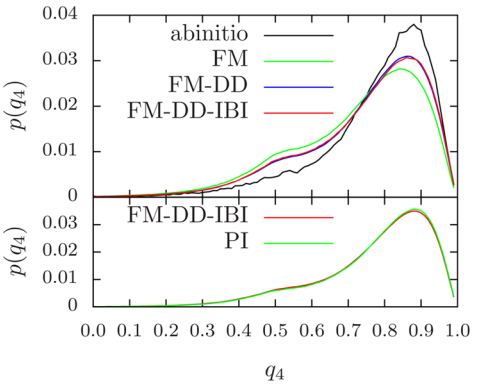

Figure 5. Comparison of the terahedral oder parameter distribution q_4. The top panel shows the comparison for D_2O at T = 325 K, the reference temperature of the abinition simulation. In the bottom, the comparison for H_2O at T = 300 K in classical and PI MD simulation is shown.

observed, whereas the FM simulations show a secondary peak/shoulder. In the original paper, Errington and Debenedetti[45] report that the relative height of the two peaks changes with the temperature: more specifically, at low temperatures the peak at higher (lower) q_4 is larger (smaller). In our first-principles simulation, the tetrahdral arrangement is more pronounced, which may be associated with the aforementioned over-structuring problem. It is therefore interesting to see that the simulations based on the FM force field produce a more "liquid-like" q_4 distribution with a higer peak at lower q_4. A possible explanation is that multibody effects missing in the FM-nonbonded potential are responsible for the high q_4 values observed in the first-principles simulation.

The virial pressure in the classical FM-DD-IBI simulation of heavy water at ρ = 1.1 g/cm^3 was found to be p = 3170 ± 20 bar, which compares well to $p \approx$ 2500 bar, estimated for water at ambient temperature by first-principles MD using the PBE density functional.[46] Therefore, our water model displays the same shortcoming of the reference model, i.e., a largely underestimated equilibrium density under ambient conditions. It is however worth noting that such agreement can be

dx.doi.org/10.1021/ct4010504 | J. Chem. Theory Comput. 2014, 10, 816−824

fortuitous, since the reference pressure is not explicitly taken into account in the FM technique as an optimization parameter. A method in which also the pressure is a target property of the CG model has been proposed by Izvekov and Voth;[41] a possible alternative to match the pressure is to introduce pressure corrections in the IBI method.[32,47] Yet, reproducing the reference pressure is out of the scope of the present work.

3.2. Dynamical Properties. Once we have verified that the structural properties of the reference system are reasonably well reproduced by the FM-DD-IBI interactions, we focused on the dynamical properties of our water model, namely the vibrational spectrum and the self-diffusion coefficient. To this end, we performed short classical MD runs (10^6 MD steps, with Δt = 0.1 fs) in the microcanonical ensemble. The vibrational density of states $I(\omega)$ is calculated from the velocity autocorrelation function of the deuterium atoms according to the relation:

$$I(\omega) = \frac{1}{N_D}\int_{-\infty}^{\infty} dt\ e^{-i\omega t} \sum_{i=1}^{N_D} \langle \mathbf{v}_i^D(t)\cdot\mathbf{v}_i^D(0)\rangle \qquad (17)$$

where N_D denotes the number of deuterium atoms in the system and $\mathbf{v}_i^D(t)$ is the velocity of atom i at time t. The resulting spectrum is shown in Figure 6, where it is compared to the spectrum calculated directly from the first-principles trajectory.

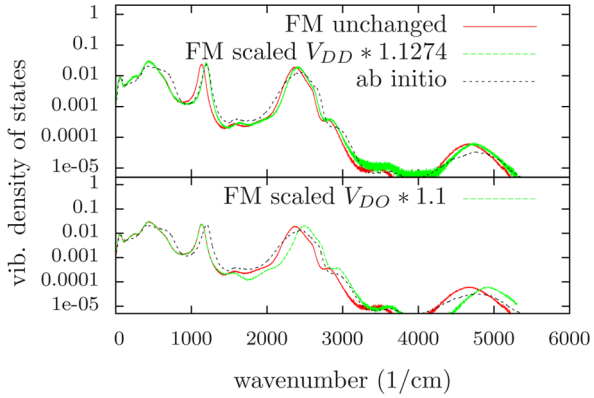

Figure 6. Density of states for the FM-DD-IBI water model and the effect of artificially scaling the intramolecular interactions: (top) scaling the D−D bond and angle interactions by k' = 1.1274 and (bottom) scaling the D−O interaction by k' = 1.1.

Also in this case, we observe a satisfactory agreement between our classical force field and the reference (see Figure 6). In particular, the broad peak at ∼2000−2700 cm^{-1} related to the D−O stretching mode is quantitatively well reproduced. The shape of the stretching band represents a major improvement over standard flexible point-charge water models.[7,48,49] The complex shape of the broad D−O stretching band of water is indeed the result of several concerted electronic intermolecular and intramolecular interactions, which also reflect the hydrogen bonding environment of water.[50−55] It is remarkable, and not obvious at all, that a relatively simple model like the one proposed here can reproduce the shape of the D−O stretching band. This indicates that the FM model can effectively account for the electronic effects explicitly included in the first-principles MD simulations by solving the electronic structure problem at high computational cost. The power spectrum in Figure 6 also displays a broad band with very low intensity at high frequency (∼4000−5000 cm^{-1}), outside the range of the normal modes of heavy water. This signal appears both in the first-principles power spectrum and in the one obtained using the FM potential, and it is most likely a second-harmonic of the D−O stretching band.

The D−O−D bending mode at ∼1050−1200 cm^{-1} is slightly red-shifted with respect to the first-principles reference. This discrepancy can be corrected by rescaling the D−O−D angular potential. We have performed an additional simulation, in which the bonded angular potential $V_\theta(\theta_{DOD})$ is rescaled by a factor k', defined as $k' = \omega_{\text{ab-initio}}^2/\omega_{FM}^2 = 1.1274$. The spectrum obtained from this simulation shows a bending frequency with exactly the first-principles frequency, leaving the remainder of the spectrum unaffected (shown in Figure 6 top), thus indicating that the bending mode is not coupled to the other vibrational modes of the system. From this observation, we can argue that the internal D−D interaction is slightly underestimated in the FM-DD-IBI, most likely due to the aforementioned fact that the bonded and nonbonded parts of the D−D distributions overlap. Analogously, it is also possible to rescale the intramolecular D−O bonding potential, V_{DO}. In a simulation in which the V_{DO} is scaled with an arbitrarily chosen factor k' = 1.1, the stretching peak shifts to higher wavenumbers, along with the peak at ∼4000−5200 cm^{-1}, leaving the rest of the spectrum unaffected. This suggests that also the stretching mode is decoupled from the rest of the vibrational spectrum and confirms that the high frequency band at ∼4000−5200 cm^{-1} is an overtone of the D−O stretching band.

The diffusion constant was calculated from the mean square displacement over time, obtained from an NVE simulation of 1 ns at room temperature (300 K) with the FM-DD-IBI forces, but the deuterium masses replaced by the appropriate value m = 1.008 au for light water (H_2O). The self-diffusion constant was found to be $D = 2.58 \times 10^{-9}$ m^2/s (see Figure 7), which is

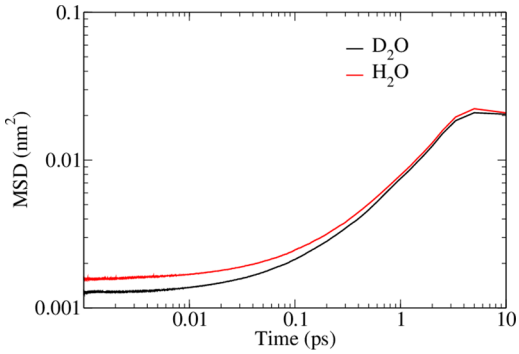

Figure 7. Mean square displacement (MSD) of light and heavy water. The diffusion coefficient of light water as calculated from the MSD is $D = 2.6 \times 10^{-9}$ m^2/s, to be compared to the experimental value $D_{exp} = 2.2 \times 10^{-9}$ m^2/s.

slightly higher than the experimental value of $D_{exp} = 2.3 \times 10^{-9}$ m^2/s (measured at T = 298 K in ref 56). The good agreement of the diffusion constants shows that the effective forces also capture the long-time dynamical properties of the system.

3.3. Nuclear Quantum Effects. Having validated our classical model on the structural and vibrational properties in the first-principles simulation of heavy water, we investigated what role, if any, the explicit inclusion of nuclear quantum

dx.doi.org/10.1021/ct4010504 | J. Chem. Theory Comput. 2014, 10, 816−824

effects plays in our model of light water, H_2O. Here, we rely on the assumption that the first-principles MD simulation of D_2O, used to fit the FM-DD-IBI classical model, sampled a sufficient portion of the phase space, so that the FM-DD-IBI is sufficiently transferable to quantum simulations of light water. We performed PIMD simulations using the FM-DD-IBI potential for 324 molecules employing 32 beads per ring. The temperature was controlled using a Langevin thermostat (τ_{Langevin} = 2 ps) coupled to all beads, so to circumvent shortcomings related to nonergodicity in sampling the modes of the PI ring polymer.[57] The simulation was run at T = 300 K, using a time step of Δt = 0.5 fs for a total of 800 ps. The initial configuration was created by choosing an equilibrated snapshot from the classical (D_2O) simulation, where every classical atom was replaced by a ring polymer with radius r^0 = 0.01 nm in the xy plane. For equilibration, short simulations using a strong coupling (τ_{Langevin} = 0.2 ps) were performed to relax the PI beads into a globular configuration. The pressure in the PI simulations, computed using the primitive pressure estimator,[58] was found to be p = 3577 ± 81 bar, which represents an increase of $\Delta p \approx$ 400 bar with respect to the pressure in the classical MD simulation at the same temperature. This increase, due to the nuclear quantum effect, is in agreement with former studies that reported an increased equilibrium density when simulating water in the constant pressure (NPT) ensemble.[7]

To compare the path integral results to the corresponding classical setup on equal footing, also classical simulations using the FM-DD-IBI potential of light water at T = 300 K were performed; the resulting data are shown in Figure 9. In the PI simulation, we observe a softening of the structure with respect to the classical simulation, most pronounced for the intramolecular peaks of the radial distribution functions. The agreement with experimental structural properties improves significantly for the H−H and H−O radial distribution functions. On the other hand, the intermolecular distributions are much less affected by quantum effects, as it is visible in the O−O radial distribution function. Similarly, the tetrahedral order of the liquid is essentially unaffected by the path integral description of the nuclei, see the bottom panel of Figure 5. These results lead us to the conclusion that the explicit inclusion of nuclear quantum effects by means of the PI method does not significantly improve the overstructuring which is commonly found in first-principles simulations relying on semilocal generalized-gradient approximation functionals.[22]

A second, more sentitive structural parameter has been recently incroduced by Ceriotti et al.[59] to quantify the propensity of a water molecule's hydrogen to detach from its bonded oxygen toward the acceptor. This proton transfer coordinate is defined as

$$\nu = d(\text{O}-\text{H}) - d(\text{O}'-\text{H}) \tag{18}$$

where d denotes the distance between a hydrogen H to the bonded oxygen O, and O′ is a neighboring molecule's oxygen. The probability distribution of ν measures to what extent the hydrogen stretches out toward the acceptor oxygen; the probability $p(\nu = 0)$ can then be seen as the likelihood for a transient autoprotolysis event. In ref 59, it has been shown that a quantum description of the nuclei greatly enhances the likelihood of transient autoprotolysis events at room temperature in first-principles MD simulation. The same behavior was not observed in PI simulations with popular empirical force fields, which show a probability $p(\nu = 0)$ several orders of magnitude lower.[59] It is therefore interesting to investigate whether our model can caputure this effect. Figure 8 shows the distribution of ν calculated from classical and PI simulations:

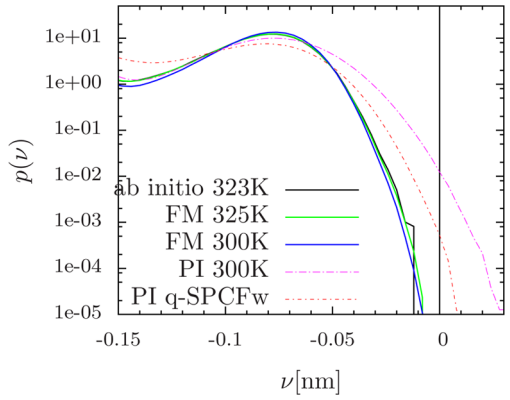

Figure 8. Proton transfer parameter as defined in ref 59, corresponding to the probability distribution of a water molecule's hydrogen nucleus along the axis between the oxygen it is bound to and the acceptor oxygen; for ν = 0, the hydrogen is in the middle point between the oxygens.

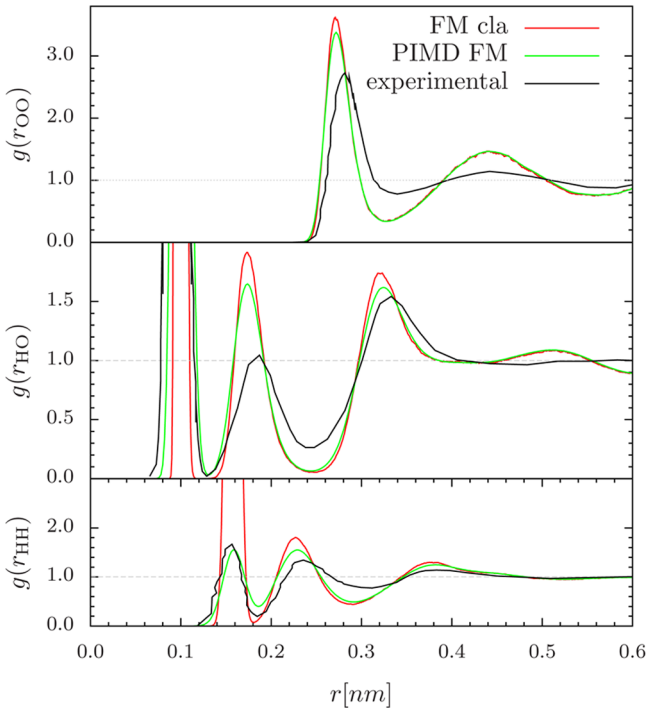

Figure 9. Radial distribution function of FM-DD-IBI at 300 K for light water without (cla) and with inclusion of the nuclear quantum effects (PIMD). Intramolecular correlations are included. Experimental data were taken from ref 61.

the FM-DD-IBI force field in the classical setup reproduces very well the distribution of the first-principles simulation; the likelihood for ν = −0.01 nm can be estimated, by extrapolation, to be $\sim 10^{-5}$. In our first principles as well as classical simulations, hydrogens never cross the middle point between the covalently bonded oxygen and the hydrogen-bonded one (ν < 0). With the introduction of a quantum description of the nuclei the probability distribution acquires a relevant component in the ν > 0 sector, and the probability in the middle point raises to $\sim 10^{-3}$, in agreement with the results by Ceriotti et al.[59] We verified that a popular model of water,

dx.doi.org/10.1021/ct4010504 | J. Chem. Theory Comput. 2014, 10, 816−824

designed for quantum simulations, namely the q-SPCFw[7] model, shows a similar behavior when used in a PI description, but the value of the probability distribution for $\nu = 0$ is 1 order of magnitude smaller than the one obtained with the FM-DD-IBI force field. We conclude that our approach is able to accurately reproduce the transient autoprotolysis of water with a clear advantage over standard empirical force fields. Such improvement probably stems from the anharmonic functional form of the OH bonded potential and is consistent with the finding that our model also accurately reproduces the vibrational dynamics of water, as discussed in the Dynamical Properties section.

We conclude our study of the nuclear quantum effects in water discussing the vibrational spectrum obtained performing an adiabatic centroid MD simulation,[34] a method briefly described in the Path Integral Formalism section. We ran a 5 ps ACMD simulation with adiabaticity parameter $\gamma = 0.15$ and a time step $\Delta t = 0.1$ fs; the noncentroid modes were thermostated with a Langevin thermostat of characteristic time $\tau_{\text{Langevin}} = 2.0$ ps at $T = 300$ K. The density of states as obtained from the centroid velocity autocorrelation function is reported in Figure 10 and compared to the corresponding

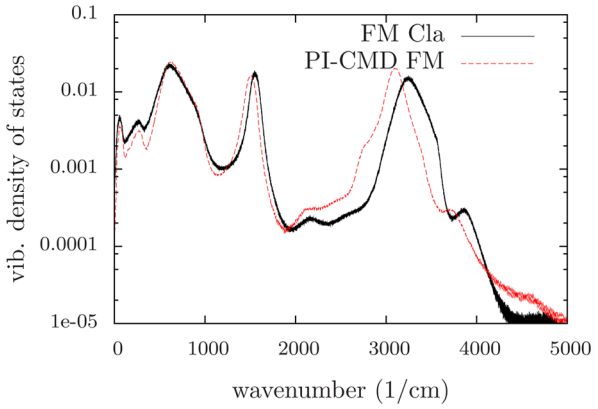

Figure 10. Density of states of classical light water (FM cla) and the corresponding spectrum obtained from ACMD (PI-CMD FM).

classical counterpart. The main features of the dynamics are retained by the PI description of the nuclei. The first (diffusion) peak is largely unaffected by the approximate quantum dynamics; in contrast, a shift to lower wavenumbers can be observed for the bending ($\Delta\omega = -44$ cm^{-1}) and stretching peaks ($\Delta\omega = -245$ cm^{-1}), in particular for the latter: this behavior can be attributed to the softening of the H−O interaction induced by the zero-point motion of the hydrogens. These results are compatible with previous observations of the red-shift in the H−O bond[60] and further validate the viability of the present water model, as even delicate dynamical quantum properties are correctly reproduced.

4. CONCLUSIONS

In summary, we have developed a systematic approach to generate a computationally efficient water model fitted on first-principles simulations, and we have validated it for the case of bulk water. The empirical force field, made of short-ranged tabulated interactions obtained by force-matching and refined using IBI, retains the structural and dynamical properties of first-principles water, specifically the complex pattern of the vibrational density of states. This indicates that the electronic effects that determine the fast dynamics of water are effectively embedded in the empirical force field.

The approach presented in this work is particularly well suited to study nuclear quantum effects, since the parametrization is directly performed on *ab initio* simulations in which the ionic dynamics is classical, but the simplicity of the empirical model allows PI and ACMD simulations, scaling to large size and long time scales.

The simulations performed employing our force field together with a quantum description of the nuclei show that the overstructuring of water from DFT-based MD simulations with respect to experiments is only marginally reduced when the quantum nature of protons is properly taken into account. These discrepancies most likely stem from the approximations entailed in the exchange and correlation functional, in our case PBE. To significantly improve the description of water, better functionals including nonlocal exchange and dispersion forces would be needed.[62,63] On the other hand, our force field reproduces with remarkable accuracy the probability distribution of the proton transfer parameter introduced by Ceriotti et al. and shows that with the PI description of the nuclei the transient autoprotolysis probability has a much larger increase than that of other standard water force fields.

In perspective, the approach described here can be applied to a large variety of cases in which it is essential to explicitly take into account the quantum nature of water, for example molecular orientation and dynamics of surface water,[64] the solvation shell of ions,[65] and water adlayers on metallic interfaces,[66−70] provided that a proper validation in the case of heterogeneous environments has been performed. In conclusion, we emphasize that the approach is completely general and can be applied to obtain reliable and computationally efficient models of a broad spectrum of soft matter systems.

■ ASSOCIATED CONTENT

Supporting Information

Supporting Information contains the tabulated potentials and forces reported in Figure 1. This material is available free of charge via the Internet at http://pubs.acs.org/.

■ AUTHOR INFORMATION

Corresponding Authors

*E-mail: potestio@mpip-mainz.mpg.de.
*E-mail: donadio@mpip-mainz.mpg.de.

Notes

The authors declare no competing financial interest.

■ ACKNOWLEDGMENTS

We are indebted to Michele Ceriotti for several helpful suggestions and to Tanja Kling and Debashish Mukherji for critical reading of the manuscript. We acknowledge the use of the computational resources provided by the Rechenzentrum Garching (RZG) of the Max Planck Society.

■ REFERENCES

(1) Kuharski, R. A.; Rossky, P. J. *J. Chem. Phys.* **1985**, *82*, 5164−5177.
(2) Paesani, F.; Voth, G. A. *J. Phys. Chem. B* **2009**, *113*, 5702−5719.
(3) Chen, B.; Ivanov, I.; Klein, M. L.; Parrinello, M. *Phys. Rev. Lett.* **2003**, *91*, 215503.
(4) Abascal, J. L. F.; Vega, C. *J. Chem. Phys.* **2005**, *123*, 234505.
(5) Berendsen, H. J. C.; Grigera, J. R.; Straatsma, T. P. *J. Phys. Chem.* **1987**, *91*, 6269−6271.

(6) Wu, Y.; Tepper, H. L.; Voth, G. A. *J. Chem. Phys.* **2006**, *124*, 024503.
(7) Paesani, F.; Zhang, W.; Case, D. A.; Cheatham, T. E.; Voth, G. A. *J. Chem. Phys.* **2006**, *125*, 4507.
(8) Habershon, S.; Markland, T. E.; Manolopoulos, D. E. *J. Chem. Phys.* **2009**, *131*, 4501.
(9) Xantheas, S. S.; Burnham, C. J.; Harrison, R. J. *J. Chem. Phys.* **2002**, *116*, 1493−1499.
(10) Burnham, C. J.; Li, J.; Xantheas, S. S.; Leslie, M. *J. Chem. Phys.* **1999**, *110*, 4566−4581.
(11) Fanourgakis, G. S.; Schenter, G. K.; Xantheas, S. S. *J. Chem. Phys.* **2006**, *125*, 1102.
(12) Paesani, F.; Iuchi, S.; Voth, G. A. *J. Chem. Phys.* **2007**, *127*, 4506.
(13) Fanourgakis, G. S.; Xantheas, S. S. *J. Chem. Phys.* **2008**, *128*, 074506−074506−11.
(14) Bukowski, R.; Szalewicz, K.; Groenenboom, G. C.; van der Avoird, A. *Science* **2007**, *315*, 1249−1252.
(15) Wang, Y.; Huang, X.; Shepler, B. C.; Braams, B. J.; Bowman, J. M. *J. Chem. Phys.* **2011**, *134*, 094509.
(16) Leforestier, C.; Szalewicz, K.; van der Avoird, A. *J. Chem. Phys.* **2012**, *137*, 014305.
(17) Babin, V.; Medders, G. R.; Paesani, F. *J. Phys. Chem. Lett.* **2012**, *3*, 3765−3769.
(18) Marx, D.; Parrinello, M. *J. Chem. Phys.* **1996**, *104*, 4077.
(19) Tuckerman, M. E.; Marx, D.; Klein, M. L.; Parrinello, M. *J. Chem. Phys.* **1996**, *104*, 5579.
(20) Marx, D.; Tuckerman, M. E.; Hutter, J.; Parrinello, M. *Nature* **1999**, *397*, 601−604.
(21) Tuckerman, M. E.; Marx, D.; Parrinello, M. *Nature* **2002**, *417*, 925−929.
(22) Morrone, J.; Car, R. *Phys. Rev. Lett.* **2008**, *101*, 017801.
(23) Badyal, Y.; Saboungi, M.; Price, D.; Shastri, S.; Haeffner, D.; Soper, A. *J. Chem. Phys.* **2000**, *112*, 9206−9208.
(24) Soper, A.; Benmore, C. *Phys. Rev. Lett.* **2008**, *101*, 065502.
(25) Skinner, L. B.; Huang, C.; Schlesinger, D.; Pettersson, L. G. M.; Nilsson, A.; Benmore, C. J. *J. Chem. Phys.* **2013**, *138*, 074506.
(26) Sovago, M.; Campen, R. K.; Wurpel, G. W. H.; Muller, M.; Bakker, H. J.; Bonn, M. *Phys. Rev. Lett.* **2008**, *100*, 173901.
(27) Tielrooij, K. J.; Garcia-Araez, N.; Bonn, M.; Bakker, H. J. *Science* **2010**, *328*, 1006−1009.
(28) Zhang, Z.; Piatkowski, L.; Bakker, H. J.; Bonn, M. *Nature Chem.* **2011**, *3*, 888−893.
(29) Mashaghi, A.; Partovi-Azar, P.; Jadidi, T.; Anvari, M.; Jand, S. P.; Nafari, N.; Tabar, M. R. R.; Maass, P.; Bakker, H. J.; Bonn, M. *J. Phys. Chem. C* **2013**, *117*, 510−514.
(30) Izvekov, S.; Parrinello, M.; Burnham, C. J.; Voth, G. A. *J. Chem. Phys.* **2004**, *120*, 10896.
(31) Car, R.; Parrinello, M. *Phys. Rev. Lett.* **1985**, *55*, 2471−2474.
(32) Reith, D.; Pütz, M.; Müller-Plathe, F. *J. Comput. Chem.* **2003**, *24*, 1624−1636.
(33) Perdew, J. P.; Burke, K.; Ernzerhof, M. *Phys. Rev. Lett.* **1996**, *77*, 3865−3868.
(34) Cao, J.; Voth, G. A. *J. Chem. Phys.* **1994**, *100*, 5106−5117.
(35) VandeVondele, J.; Krack, M.; Mohamed, F.; Parrinello, M.; Chassaing, T.; Hutter, J. *Comput. Phys. Commun.* **2005**, *167*, 103−128.
(36) VandeVondele, J.; Hutter, J. *J. Chem. Phys.* **2007**, *127*, 114105−114105−9.
(37) Bussi, G.; Donadio, D.; Parrinello, M. *J. Chem. Phys.* **2007**, *126*, 014101.
(38) Grossman, J.; Schwegler, E.; Draeger, E.; Gygi, F.; Galli, G. *J. Chem. Phys.* **2004**, *120*, 300−311.
(39) KuÌLhne, T. D.; Krack, M.; Parrinello, M. *J. Chem. Theory Comput.* **2009**, *5*, 235−241.
(40) Ercolessi, F.; Adams, J. B. *Europhys. Lett.* **1994**, *26*, 583−588.
(41) Izvekov, S.; Voth, G. A. *J. Phys. Chem. B* **2005**, *109*, 2469−2473.
(42) Noid, W. G.; Chu, J.-W.; Ayton, G. S.; Krishna, V.; Izvekov, S.; Voth, G. A.; Das, A.; Andersen, H. C. *J. Chem. Phys.* **2008**, *128*, 244114.
(43) Rühle, V.; Junghans, C.; Lukyanov, A.; Kremer, K.; Andrienko, D. *J. Chem. Theory Comput.* **2009**, *5*, 3211−3223.
(44) Feynman, R. P.; Hibbs, A. R. *Quantum Mechanics and Path Integrals*; McGraw-Hill: New York, 1965; pp 267−296.
(45) Errington, J. R.; Debenedetti, P. G. *Nature* **2001**, *409*, 318−321.
(46) Yoo, S.; Zeng, X. C.; Xantheas, S. S. *J. Chem. Phys.* **2009**, *130*, 221102−221102−4.
(47) Wang, H.; Junghans, C.; Kremer, K. *Eur. Phys. J. E: Soft Matter Biol. Phys.* **2009**, *28*, 221−229.
(48) Dang, L. X.; Pettitt, B. M. *J. Phys. Chem.* **1987**, *91*, 3349−3354.
(49) Gordillo, M. C.; Nagy, G.; Mart, J. *J. Chem. Phys.* **2005**, *123*, 054707.
(50) Auer, B. M.; Skinner, J. L. *J. Chem. Phys.* **2008**, *128*, 224511.
(51) Corcelli, S.; Lawrence, C.; Skinner, J. *J. Chem. Phys.* **2004**, *120*, 8107−8117.
(52) Geissler, P. *J. Am. Chem. Soc.* **2005**, *127*, 14930−14935.
(53) Donadio, D.; Cicero, G.; Schwegler, E.; Sharma, M.; Galli, G. *J. Phys. Chem. B* **2009**, *113*, 4170−4175.
(54) Zhang, C.; Donadio, D.; Galli, G. *J. Phys. Chem. Lett.* **2010**, *1*, 1398−1402.
(55) Zhang, C.; Donadio, D.; Gygi, F.; Galli, G. *J. Chem. Theory Comput* **2011**, *7*, 1443−1449.
(56) Holz, M.; Heil, S. R.; Sacco, A. *Phys. Chem. Chem. Phys.* **2000**, *2*, 4740−4742.
(57) Hall, R. W.; Berne, B. J. *J. Chem. Phys.* **1984**, *81*, 3641.
(58) Tuckerman, M. *Statistical Mechanics: Theory and Molecular Simulation*; Oxford University Press: Oxford, U. K., 2010; pp 456−461.
(59) Ceriotti, M.; Cuny, J.; Parrinello, M.; Manolopoulos, D. E. *Proc. Natl. Acad. Sci. U. S. A.* **2013**, *110*, 15591−15596 (PMID: 24014589).
(60) Paesani, F.; Voth, G. A. *J. Chem. Phys.* **2010**, *132*, 014105.
(61) Soper, A. *Chem. Phys.* **2000**, *258*, 121−137.
(62) Santra, B.; Michaelides, A.; Scheffler, M. *J. Chem. Phys.* **2007**, *127*, 184104.
(63) Santra, B.; Michaelides, A.; Fuchs, M.; Tkatchenko, A.; Filippi, C.; Scheffler, M. *J. Chem. Phys.* **2008**, *129*, 194111.
(64) Nagata, Y.; Pool, R. E.; Backus, E. H. G.; Bonn, M. *Phys. Rev. Lett.* **2012**, *109*, 226101.
(65) Tielrooij, K. J.; Garcia-Araez, N.; Bonn, M.; Bakker, H. J. *Science* **2010**, *328*, 1006−1009.
(66) Walker, B.; Michaelides, A. *J. Chem. Phys.* **2010**, *133*, 174306.
(67) Li, X.-Z.; Probert, M. I. J.; Alavi, A.; Michaelides, A. *Phys. Rev. Lett.* **2010**, *104*, 066102.
(68) Carrasco, J.; Santra, B.; Klimes, J.; Michaelides, A. *Phys. Rev. Lett.* **2011**, *106*, 026101.
(69) Li, X.-Z.; Walker, B.; Michaelides, A. *Procs. Natl. Acad. Sci. U. S. A.* **2011**, *108*, 6369−6373.
(70) Donadio, D.; Ghiringhelli, L.; Delle Site, L. *J. Am. Chem. Soc.* **2012**, *134*, 19217−19222.